remote sensing

MDPI

Article

A Random Forest Model for Drought: Monitoring and Validation for Grassland Drought Based on Multi-Source Remote Sensing Data

Qian Wang [1], Lin Zhao [1], Mali Wang [1], Jinjia Wu [2], Wei Zhou [3], Qipeng Zhang [1,*] and Meie Deng [4]

[1] Department of Geographic Information Science, School of Geography and Environment, Liaocheng University, Liaocheng 252059, China
[2] Grand Canal Research Centre, The Grand Canal Research Institute, Liaocheng University, Liaocheng 252000, China
[3] Chongqing Jinfo Mountain Karst Ecosystem National Observation and Research Station, School of Geographical Sciences, Southwest University, Chongqing 400715, China
[4] School of Management, Wuhan Polytechnic University, Wuhan 430048, China
* Correspondence: qpzhang@lcu.edu.cn

Abstract: The accuracy of drought monitoring models is crucial for drought monitoring and early warning. Random forest (RF) is being used widely in the field of artificial intelligence. Nonetheless, the application of a random forest model in grassland drought monitoring research is yet to be further explored. In this study, various drought hazard factors were integrated based on remote sensing data, including from the Moderate Resolution Imaging Spectroradiometer (MODIS) and Global Precipitation Measurement (GPM), as multisource remote sensing data. Based on the RF, a comprehensive grassland drought monitoring model was constructed and tested in Inner Mongolia, China, as an example. The critical issue addressed is the construction of a grassland drought disaster monitoring model based on meteorological data and multisource remote sensing data by using an RF model, and the verification of the accuracy and reliability of its monitoring results. The results show that the grassland drought monitoring model could quantitatively monitor the drought situation in Inner Mongolia grasslands. There was a significantly positive correlation between the drought indicators output by the model and the standardized precipitation evapotranspiration index (SPEI) measured in the field. The correlation coefficients (R) between the drought degree were 0.9706 and 0.6387 for the training set and test set, respectively. The consistent rate between the model drought index and the SPEI reached 87.90%. Drought events in Inner Mongolia were monitored from April to September in wet years, normal years, and dry years using the constructed model. The monitoring results of the model constructed in this study were in accordance with the actual drought conditions, reflecting the development and spatial evolution of drought conditions. This study provides a new application method for the comprehensive assessment of grassland drought.

Keywords: random forest; grassland drought monitoring; SPEI; drought

Citation: Wang, Q.; Zhao, L.; Wang, M.; Wu, J.; Zhou, W.; Zhang, Q.; Deng, M. A Random Forest Model for Drought: Monitoring and Validation for Grassland Drought Based on Multi-Source Remote Sensing Data. *Remote Sens.* **2022**, *14*, 4981. https://doi.org/10.3390/rs14194981

Academic Editors: Duk-jin Kim and Jinmu Choi

Received: 4 September 2022
Accepted: 27 September 2022
Published: 7 October 2022

1. Introduction

As a common natural phenomenon, drought has always been of high concern to scientists in all fields because of its processes involving various factors, such as the atmosphere, soil, and vegetation [1–3]. One of the more serious disasters on a global scale, droughts have a serious impact on the sustainable development of ecosystems because of their high frequency, wide range of effects, and long duration [4–6]. Therefore, there is a need for drought monitoring and early warning studies.

The evolution of drought disasters not only includes a complex dynamic process and a multi-scale water and energy circulation mechanism, but it also involves many fields, including meteorology, agriculture, hydrology, ecology, and social economy. There are four types of droughts—meteorological, hydrological, agricultural, and socioeconomic droughts [7–9]. Researchers have explored the evolution process of drought disasters from different perspectives [10,11]. To reduce the ecological impacts of drought disasters, numerous drought indices were used to monitor the development process from drought to drought disasters [5]. According to the Handbook of Drought Indicators and Indices, there are three main methods for monitoring drought and guiding early warning and assessment: (1) using a single indicator, (2) using multiple indicators, and (3) using composite indicators [12]. Single-indicator drought monitoring relies on stations that measure certain parameters to help identify drought, including meteorological stations, agrometeorological stations, and hydrological stations. The accuracy of drought monitoring using stations is relatively high. However, due to the limitation of the number of stations and the uneven spatial distribution, single-indicator drought monitoring cannot achieve large-scale drought disaster monitoring. Remote sensing can reveal drought conditions by the inversion of soil moisture or vegetation growth over large areas. However, drought monitoring results by monitoring vegetation growth or soil water content do not reflect the drought mechanisms. Multiple indicators have been constructed based on station data and remote sensing data for drought monitoring. There has been strong global interest and growth in the development of new indices based on various indicators that are suitable for different applications and scales, both spatial and temporal. With the rapid advance of computer technology and the "Internet Plus", human beings have entered the era of big data. The rise of new technologies, including data mining, cloud computing, etc., has driven the progress of drought disaster monitoring research. Drought monitoring models have been obtained by combining station data and remote sensing data based on weighting or modeling methods to combine different drought indicators, named composite indicators by the World Meteorological Organization (WMO) [12]. Many scholars have attempted to assign weight coefficients to construct linear weighted combination models to monitor regional drought disasters [13,14]. For instance, some scholars constructed the normalized agricultural drought composite index (SDCI) by assigning different weights to the normalized vegetation index (NDVI), TRMM precipitation data, and surface temperature index (LST). Others constructed the decadal-scale crop drought monitoring model (MNDVI) by assigning a 0.5 weight to the TRMM precipitation data and NDVI values. Other researchers selected the precipitation index (PCI), GLDAS soil moisture data, TCI, and VCI to construct multiple linear regression indices (MCDIs). These studies have provided ideas for integrated drought disaster monitoring, but the weight values in linear regression model construction need to be obtained after several trials. Thus, the linear regression model construction process is influenced by human experience. Some scholars have tried to apply data mining methods to drought disaster monitoring studies [5,15] and have constructed numerous integrated drought monitoring models [16–18]. for example, the vegetation drought response index (VegDRI) using categorical regression trees, the integrated surface drought index (ISDI), the multivariate standardized drought index (MSDI), and the meteorological agricultural integrated drought index (MMSDI) based on MSDI. These studies have provided new ideas and perspectives for drought disaster monitoring research. However, the complex linkages among the data from different sources and their inconsistencies at spatial and temporal scales also pose a greater challenge for drought monitoring. Thus, it is necessary to introduce new algorithms for drought monitoring and early warning research.

Random forest (RF) was proposed by Breiman in 2001. RF is the association between multiple branchless pruned classification and regression trees (CARTs), which is an evolution and development of the traditional decision tree method [19,20]. RF constructs a decision tree using a random decision method, which reduces some of the random errors in the classification regression process and improves the accuracy of the classification regression results [21,22]. RF inherits and develops the advantages of traditional decision tree methods and does not suffer from overfitting problems. Moreover, the RF model is a nonlinear ensemble learning technique with high simulation accuracy and a highly flexible model-building process. In addition, it does not involve the problem of multicollinearity between independent variables that needs to be solved in a regression model. RF has been widely used in ecological and environmental fields because of its fast computational speed and good stability compared to the linear regression algorithm and the neural network algorithm. RF can input multiple variables, is highly stable for variations in classification model parameter values, and averages the predictions for individual trees in the forest. As a result, the RF has advantages in classification and prediction [23,24]. Thus, RF has been applied to agricultural drought disaster monitoring. However, the application of the random forest model in grassland drought monitoring has been less studied. Therefore, there is a need to conduct research on the application of the random forest model in grassland drought monitoring.

Grassland ecosystems, which are an essential part of terrestrial ecosystems, play an important role in maintaining regional and national ecological security as well as the global ecological environment [25,26]. The frequency of droughts and the areas affected by droughts are still increasing with global change. Drought is a significant climatic disturbance in grasslands. The Inner Mongolia grassland is located in northern China, spanning arid and semi-arid regions, and is an important part of the grasslands of Eurasia. As the most extensive grassland in China, the Inner Mongolia grassland is a barrier to China's ecological security [27]. The RF has good applicability and practicality in agricultural drought disaster monitoring [15]. Thus, in this study, we introduced the random forest model for grassland drought disaster monitoring and early warning.

With global climate change, fast and effective drought monitoring is an important theoretical basis for drought prevention and drought relief for grasslands. The specific objectives of this study were to construct an application model for monitoring and early warning of grassland drought hazards based on the random forest algorithm and to validate the monitoring results of the model. The main issues addressed in this study are: (a) the construction of a grassland drought monitoring model using the meteorological station data and remote sensing data based on random forest, (b) the verification of the accuracy and reliability of the monitoring results of the grassland drought monitoring model. The results provide some theoretical and technical support for grassland drought disaster monitoring and early warning.

This paper is organized as follows. The materials and methods are briefly described in Section 2. The construction of the drought monitoring model is described in Section 3. The model calibration and validation and some conclusions are outlined in Section 4 and the final section, respectively.

2. Materials and Methods

2.1. Study Area Description

The Inner Mongolia Autonomous Region, abbreviated as Inner Mongolia, is located in the interior of the Eurasian continent and the southern part of the Mongolian Plateau (97°12′~126°04′E and 37°24′~53°23′N). As an important natural grassland, the Inner Mongolia grassland is the main component of the northern grassland in China. Its total area is approximately 86.67×10^4 km^2, accounting for more than 27% of the total grassland area in China, of which the available grassland area is approximately 68.18×10^4 km^2 [28–30]. The average annual temperature ranges from −3.0 to 6.7 °C. The mean annual precipitation is about 150 to 450 mm, characterized by a decreasing trend from east to west. The precipitation is mainly concentrated between July and September [31]. Due to the complex and changing geographical and climatic conditions, the grasslands of Inner Mongolia are extremely vulnerable to natural disasters, especially drought disasters. The drought evolution of the Inner Mongolia grassland was characterized by multiple timescales, with a 17-year timescale as the primary period [31]. The land use types in Inner Mongolia include cultivated land, forest, grassland, shrubland, wetland, water bodies, artificial surface, and bare land (Figure 1).

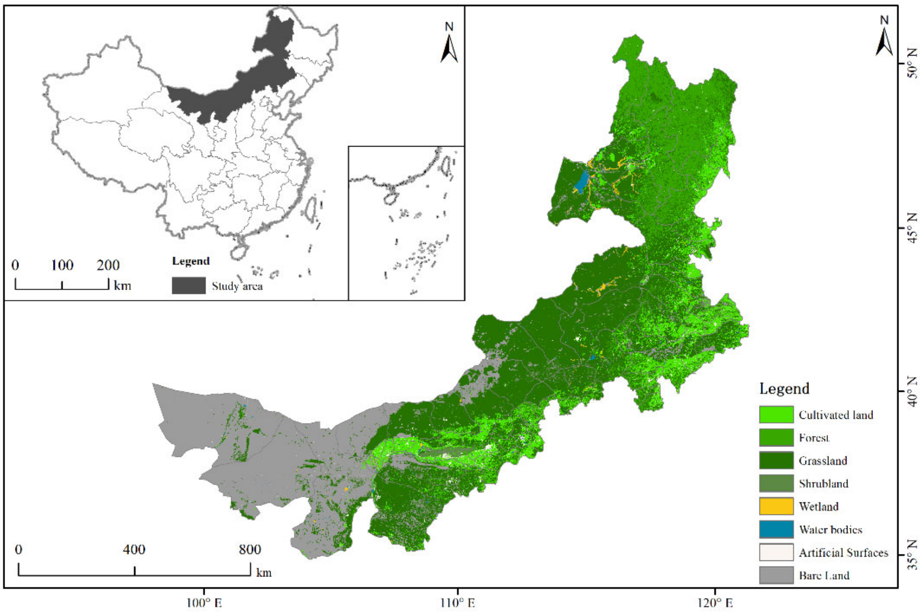

Figure 1. Location and use distribution map of the study area.

2.2. Data Sources and Processing

2.2.1. Meteorological Data

The meteorological data utilized in this study include the monthly average temperature, monthly maximum temperature, monthly minimum temperature, monthly precipitation data, wind speed data at 2 m height, station altitude, station longitude, and sunshine hours (h) from 39 major meteorological stations during 2001–2018 in Inner Mongolia. We downloaded these data from the website (http://data.cma.cn/detail/dataCode/A.0012.0001.html, accessed on 26 September 2022). The data quality needed to be checked and supplemented due to missing data from some meteorological stations. We interpolated the missing data by linear regression based on data from the same month of the calendar year.

2.2.2. Remote Sensing Data

The Moderate Resolution Imaging Spectroradiometer (MODIS) enhanced vegetation index (EVI) product (MOD13A3), the Global Precipitation Measurement (GPM), and the surface temperature product (MOD11A2) were utilized as the primary remote sensing data sources from 2001 to 2018. EVI and NDVI were derived from MOD13A3, with a spatial resolution of 1km. MOD11A2 provides the daytime surface temperature product, the nighttime surface temperature product, and the associated data quality product, with a spatial resolution of 1km. The GPM-3IMERG, after data processing, is a monthly averaged grid precipitation dataset (mm/h), with a spatial resolution of $0.1^\circ \times 0.1^\circ$ covering N60°~S60°. GPM data and MODIS data are both available from the website (https://search.earthdata.nasa.gov/search?q=GPM, accessed on 26 September 2022). In addition, we also used Shuttle Radar Topography Mission Digital Elevation Model (SRTM-DEM) data that we obtained from the website (http://srtm.csi.cgiar.org/srtmdata/, accessed on 26 September 2022). The SRTM-DEM data used were from the V4.1 version of SRTM3 data, with a spatial resolution of 90 m by interpolation algorithm to fill the gaps in this study (Table 1).

2.2.3. Statistical Data

The history of drought disasters statistics and information were collected from the Yearbook of Meteorological Disasters in China and the Inner Mongolia Statistical Yearbook. To verify the adaptability of the grassland drought monitoring model, we selected wet years, normal years, and dry years for monitoring. According to the Inner Mongolia

Statistical Yearbook, 2012 was a wet year, 2015 was a normal year, and 2017 was a dry year. Therefore, we used the actual disasters of 2012, 2015, and 2017 for model validation.

Table 1. Data description and sources.

Data	Description	Source
Meteorological data	Monthly average temperature Monthly maximum/minimum temperature Precipitation data Wind speed data at 2 m height Station altitude/longitude Sunshine hours (h)	National Meteorological Information Center (http://data.cma.cn/detail/dataCode/A.0012.0001.html)
MOD13A3 (1 km)	Moderate Resolution Imaging Spectroradiometer Enhanced vegetation index product	National Aeronautics and Space Administration (https://search.earthdata.nasa.gov/search?q=GPM)
GPM-3IMERG ($0.1° \times 0.1°$)	Monthly averaged grid precipitation dataset (mm/h)	
MOD11A2 (1 km)	Surface temperature product	
SRTM3 V4.1 (90 m)	Shuttle Radar Topography Mission Digital Elevation Model	(http://srtm.csi.cgiar.org/srtmdata/)

2.3. Data Processing

2.3.1. Calculation of Standardized Precipitation Evapotranspiration Index (SPEI)

The standardized precipitation evapotranspiration index (SPEI) is calculated as the difference between the monthly precipitation and potential evapotranspiration and aggregated at different timescales [32]. The SPEI provides a more objective description of drought conditions than the drought index calculated using precipitation alone. Therefore, the SPEI is widely employed in drought monitoring at different timescales. The Penman–Monteith model recommended by the Food and Agriculture Organization of the United Nations (FAO) was used to calculate cumulative daily precipitation and cumulative potential evapotranspiration, which takes into account the effects of the regional temperature, precipitation, sunshine duration, wind speed at a 2 m height, and relative humidity of the regional water balance from 2001 to 2018. Therefore, we applied the Penman–Monteith method to calculate the SPEI. The calculation process details for the SPEI can be found in a previous study [33]. The SPEI has a multi-timescale characteristic. According to a previous study, SPEI6 has more applicability and practicability for drought monitoring in Inner Mongolia. Thus, we calculated the SPEI at 6-month timescales with the R package and expressed it as SPEI6. The SPEI drought classification is shown in Table 2.

Table 2. Classification of SPEI values.

SPEI Value Class	Situation Classification
≤ -2.0	Extreme drought
$-2.0 < \text{SPEI} \leq -1.5$	Severe drought
$-1.5 < \text{SPEI} \leq -1.0$	Moderate drought
$-1.0 < \text{SPEI} \leq -0.5$	Mild drought
$-0.5 < \text{SPEI} \leq 0.5$	Normal or wet spell

2.3.2. Processing of Remote Sensing Data

The MODIS-EVI and LST data were respectively extracted from the MOD13A3 and MOD11A2 datasets using the MODIS Reprojection Tool (MRT) provided by NASA. EVI data are monthly value synthetic data, and LST data are 8 d synthetic data. To ensure the consistency of the temporal phase of the data used for modeling, the LST data were weighted by the proportion of the 8d data for that month to obtain a monthly surface temperature index. For example, if the flat-year LST data numbers 097, 105, 113, and

121 account for 7, 8, 8, and 7 days of April, the corresponding ratios are 7/30, 8/30, 8/30, and 7/30, respectively. Before normalizing the data from EVI and LST, poor-quality image element values and invalid values needed to be removed from the images according to the data quality control file and then filled in with the average of data from the same month of other years. To ensure that precipitation data were in monthly values, it was necessary to convert the GPM-3IMERG data in hourly precipitation units to monthly precipitation units. This was calculated by multiplying the GPM-3IMERG data by 24 h and then by the number of days in the month. Finally, the EVI, LST, GPM-3IMERG, and DEM data were reprojected from the original integerized sinusoidal projection into an Albers equal-area conical projection based on the WGS-84 datum using ArcGIS V10.8 software (ESRI, Redlands, CA, USA). Moreover, we extracted the remote sensing data (EVI, LST, GPM-3IMERG, and DEM data) for the administrative boundaries of Inner Mongolia based on ArcGIS V10.8 software (ESRI, Redlands, CA, USA).

3. Drought Monitoring Model Construction

3.1. Principles of Grassland Drought Monitoring Model Construction

The precipitation status index (GPMI) index is used for information on meteorological precipitation anomalies, and the temperature status index (TCI) demonstrates the effect of surface temperature on vegetation [34]. The enhanced vegetation index (EVI) indicates the growth status of vegetation, and the slope (Aspect), and slope direction and elevation (DEM) also have significant influence on regional drought. While each factor in different aspects reflects the drought, the ways in which they are coupled with drought are still unclear. The SPEI incorporates the effects of precipitation, temperature, and surface evapotranspiration on drought, indicating precipitation anomalies at different timescales. Accordingly, a multi-source remote sensing data-driven grassland drought monitoring model was constructed using a random forest algorithm, which used the SPEI as the dependent variable and other remote sensing factors as independent variables. The overall steps in constructing the grassland drought monitoring model included data collection, data analysis, adjustment of the model parameters, and model validation (Figure 2). In this work, a composite grassland drought monitoring model was constructed.

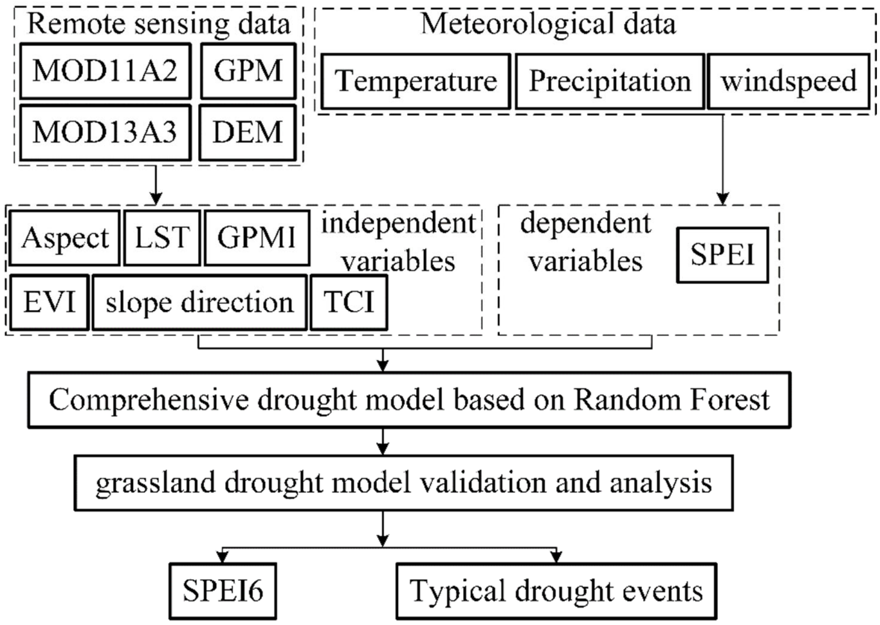

Figure 2. Grassland drought monitoring model construction.

3.2. Vegetation Condition Index

When the vegetation is under drought stress, the NDVI and EVI will decrease accordingly [35,36]. The NDVI is influenced by soil background values, and its sensitivity is low in areas with high vegetation cover [37]. In contrast, the EVI can effectively correct the influence of the background values (soil and aerosol) of the vegetation by adding blue light bands to adjust the atmospheric effect on vegetation. Furthermore, the EVI also can effectively reflect the growth of vegetation, even in areas with high vegetation cover [38]. Thus, in the model construction of this study, we selected the EVI to reflect the vegetation growth. The EVI for each month from 2001 to 2018 was calculated by the following formula:

$$\mathrm{EVI} = 2.5 * (\mathrm{NIR} - \mathrm{R}) / (\mathrm{NIR} + \mathrm{C}_1 * \mathrm{R} + \mathrm{C}_2 * \mathrm{B} + \mathrm{L}) \tag{1}$$

where NIR, R, and B denote the atmospherically corrected reflectance values in the near-infrared, red, and blue wavelengths, respectively. C_1 and C_2 are the atmospheric conditioning parameters, with values of 6.0 and 7.5, respectively. L is the soil conditioning parameter, with a value of 1.

3.3. Precipitation Condition Index (GPMI)

Drought disaster can be thought of as the result of a shortage of precipitation over a particular timescale that leads to a soil moisture deficit, limiting the water availability for vegetation. GPM data can provide monthly precipitation data, which can reflect the spatial and temporal variation of regional climate and provide meteorological drought information. Moreover, GPM data have high agreement with the measured precipitation data. Therefore, the GPMI that could reflect the precipitation on the time series was selected. To eliminate the effect between different resolutions, data normalization of the origin GPM data was required, as follows:

$$\mathrm{GPMI} = \frac{\mathrm{GPM}_{max} - \mathrm{GPM}}{\mathrm{GPM}_{max} - \mathrm{GPM}_{min}} * 100 \tag{2}$$

where GPMI represents the precipitation state index, GPM is the pixel values of precipitation, and GPM_{max} and GPM_{min} denote the maximum and minimum precipitation of the same month from 2001 to 2018, respectively. The GPMI values range from 0 to 1. The closer the GPMI value is to 0, the higher the probability of drought. Conversely, the closer the GPMI value is to 1, the more abundant regional precipitation is. In this study, the precipitation status index was calculated for each year from April to September for the period from 2001 to 2018.

3.4. Temperature Condition Index (TCI)

The soil water content will decrease with the development of drought. Drought occurrence and development are strongly correlated with the surface temperature (LST). Therefore, in years when drought occurs, the surface temperature values are higher than in the same months of normal years. The LST is influenced by atmospheric and geographical factors, so it cannot be directly used for complete drought monitoring [34]. The temperature condition index (TCI) is described based on the principle that the surface temperature of the tree canopy or soil increases with increasing temperature [39]. Under high-temperature conditions, water stress increases, resulting in a lack of water in the vegetation or soil. Thus, when vegetation is subjected to water stress, the stomata are closed to reduce transpiration, and the canopy temperature of the vegetation will increase with water stress. Moreover, the TCI is widely used in drought monitoring. Therefore, we used the TCI as one of the independent variables in the construction of the drought monitoring model.

$$\mathrm{TCI} = \frac{\mathrm{LST}_{max} - \mathrm{LST}}{\mathrm{LST}_{max} - \mathrm{LST}_{min}} * 100 \tag{3}$$

where TCI represents the temperature condition index, LST is the pixel value of the LST data, and LST_{max} and LST_{min} represent the maximum and minimum values of LST in the same month from 2001 to 2018. The values of the TCI range from 0 to 1. The smaller the TCI value, the more severe the water stress on the regional grassland growth, and the greater the possibility of regional drought. The closer the TCI value is to 0, the more serious the situation of drought in grassland. On the contrary, the closer the TCI value is to 1, the lighter the water stress is in grassland, and the lower the possibility of regional drought. In this study, the TCI was calculated for each year from April to September for the period from 2001 to 2018.

3.5. Other Factors

The spatial distribution of drought is related to regional evapotranspiration. Aspect can indirectly affect regional evapotranspiration and plant transpiration by influencing the spatial distribution of solar radiation input. The slope direction affects plant transpiration by influencing the distribution of lightness, soil temperature, soil water content, and nutrients. Evapotranspiration, precipitation, and light intensity vary spatially depending on elevation differences. Therefore, elevation factors were also used as independent variable factors in the construction process of the model.

3.6. Construction Process for a Grassland Drought Monitoring Model

Taking into account the characteristics of grassland vegetation growth, a monitoring period from April to September of each year from 2001 to 2018 was selected for this study. The growing season of the Inner Mongolia grassland is from April to September every year. To study the interaction mechanism between grassland, precipitation, and soil, a grassland drought monitoring model with SPEI = ¦ (GPMI, TCI, EVI, Aspect, slope direction, DEM) was conducted based on the random forest algorithm. The monthly SPEI is considered a dependent variable and presents the combined drought status of each station.

The precipitation state index (GPMI), temperature state index (TCI), enhanced vegetation state index (EVI), slope (Aspect), and the slope direction and elevation (DEM) of the Inner Mongolia region were used as independent variables, and SPEI6 was used as a dependent variable in the model construction.

In this study, we randomly divided the data from 2001 to 2018 into two parts: 70% were the training data and the remaining 30% were the test data. Among these, the training data were used to construct the grassland model based on the RF, and the test data were used to validate the model accuracy. Drought was identified based on the SPEI6 value and the typical drought events. The model building procedure is shown in Figure 2.

The principal steps of the construction of a model based on RF are as follows:

(1) Random repetitive sampling from the training dataset is repeated n times to generate n new training samples, while the unsampled samples constitute out-of-bag (OOB) data.
(2) Each training sample constitutes a regression tree in a random forest, and at each node of the regression tree, m variables are randomly selected from six variables for branching. The out-of-bag error is estimated based on the out-of-bag data corresponding to the training sample. The regression trees generated from the training samples constitute the random forest. The random forest prediction result is the mean of the prediction results of all regression trees. The random forest prediction accuracy is then the mean of the out-of-bag errors for all regression trees.
(3) The most important part of the model-building process is to determine the number of regression trees n and the number of preselected variables at tree nodes m. The number of m is determined in steps of 1 by looking at the value corresponding to their minimum error. In general, the number of m is not changed once it is determined. In addition, the number of m is smaller than that of the variables involved in the modeling.
(4) The number of regression trees n was determined on the basis of m. The step size of n was incremented by 100, and the default was 500. After several trials, when m = 4 and $n = 1000$, the OOB error of this study was minimized. Consequently, we finally chose the following parameters as the initial input parameters of the model: m = 4 and $n = 1000$. With such a modeling process, we explored a better model for grassland drought monitoring.

4. Results

4.1. Model Calibration and Validation

The correlation coefficient between the estimated drought index (SPEI6) for the training set and the measured SPEI6 was 0.9706, and the correlation coefficient between the estimated drought index (SPEI6) for the testing set and the measured SPEI6 was 0.6387 (Table 3). The results show that the correlation coefficients for all 39 major meteorological stations were above 0.5, and all passed the significance test of $p < 0.01$. Additionally, the RMSEs of the training set and the testing set were 0.18555 and 0.43636, respectively. Moreover, the Std values of the training set and the testing set were 0.00364 and 0.01299, respectively. Thus, the model constructed based on the RF can be used for grassland drought monitoring.

Table 3. The accuracy of the model predictions in the training and test sets.

	Standard Deviation (Std)	Root Mean Square Error (RMSE)	Correlation Coefficient (R)
Training set	0.00364	0.18855	0.9706 **
Testing set	0.01299	0.43636	0.6387 **

Note: ** is a significant correlation at the 0.01 level (two-sided).

To better verify the accuracy of the constructed model monitoring results, we classified the SPEI6 into five drought levels: extreme drought, severe drought, moderate drought, mild drought, and normal (Table 2). We also conducted drought class statistics for the actual measured and model-predicted values of SPEI6 from 2001 to 2018. The consistent rate between the measured and simulated values of drought classes was found to be 87.90%. The R^2 between the estimated SPEI value and the measured SPEI value for the training set was 0.94207, and the R^2 between the estimated SPEI value and the measured SPEI value for the testing set was 0.40741 (Figure 3). This demonstrates that the constructed model for grassland drought monitoring developed in this study had a high simulation accuracy. Thus, the constructed drought model can be used for grassland drought monitoring.

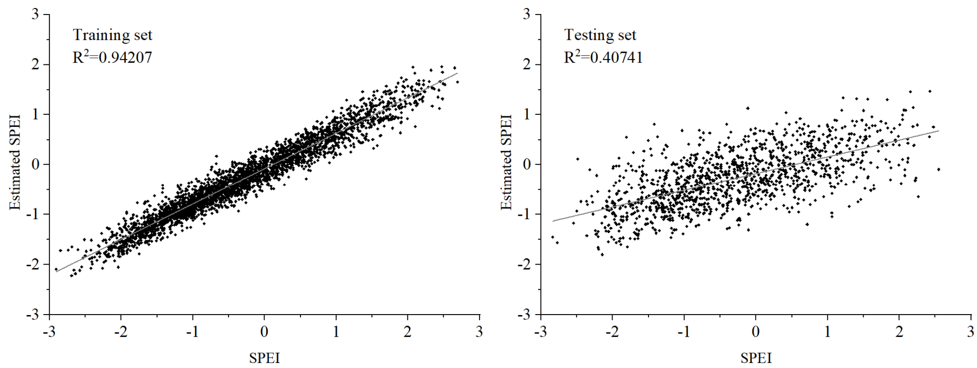

Figure 3. Correlation analysis between estimated and measured SPEI values.

4.2. Analysis of Model Monitoring Results

To verify the adaptability of the grassland drought monitoring model, we selected wet years, normal years, and dry years for monitoring. According to the Inner Mongolia Statistical Yearbook, the annual precipitation in Inner Mongolia in 2012 was 427 mm, 121 mm more than normal years, so 2012 was a wet year. In 2015, the 328 mm of annual precipitation in Inner Mongolia was close to normal years, so 2015 was a normal year. In 2017, the 282 mm of average annual precipitation was 11.5% less than in normal years, so 2017 was a dry year. Therefore, we used the actual disasters of 2012, 2015, and 2017 for model validation.

4.2.1. Analysis of Grassland Drought Monitoring Model Monitoring Results in Wet Years

From April to September 2012, the grassland drought monitoring model constructed in this study was used to monitor and classify the grassland drought in Inner Mongolia. As shown in Figure 4, there was no drought in most regions of Inner Mongolia in April. Mild drought occurred in most areas of Inner Mongolia in April, and moderate drought and severe drought appeared in central and western Hulunbeier, eastern Xing'an League, eastern Tongliao and Xilin Gol League, and Bayannur, and extreme drought appeared in some regions. In May, the severity of the drought reduced, and mild drought and no drought occurred in most areas. Inner Mongolia was largely free of extreme drought, but severe drought occurred in some areas of northeastern Hulunbeier. In general, the severity of drought increased, and mild drought and moderate drought appeared in most areas of Inner Mongolia in June. In July, the drought continued to increase in severity, with moderate drought in the central regions of Inner Mongolia. Extreme drought occurred in Hulunbeier in eastern Inner Mongolia. In August, the drought conditions intensified and resulted in severe and extreme drought over large areas in central and eastern Inner Mongolia. Moreover, severe drought spread to central and eastern parts of Inner Mongolia. In September, there was essentially no drought or mild drought in most regions, except for moderate or extreme drought in central and western Inner Mongolia.

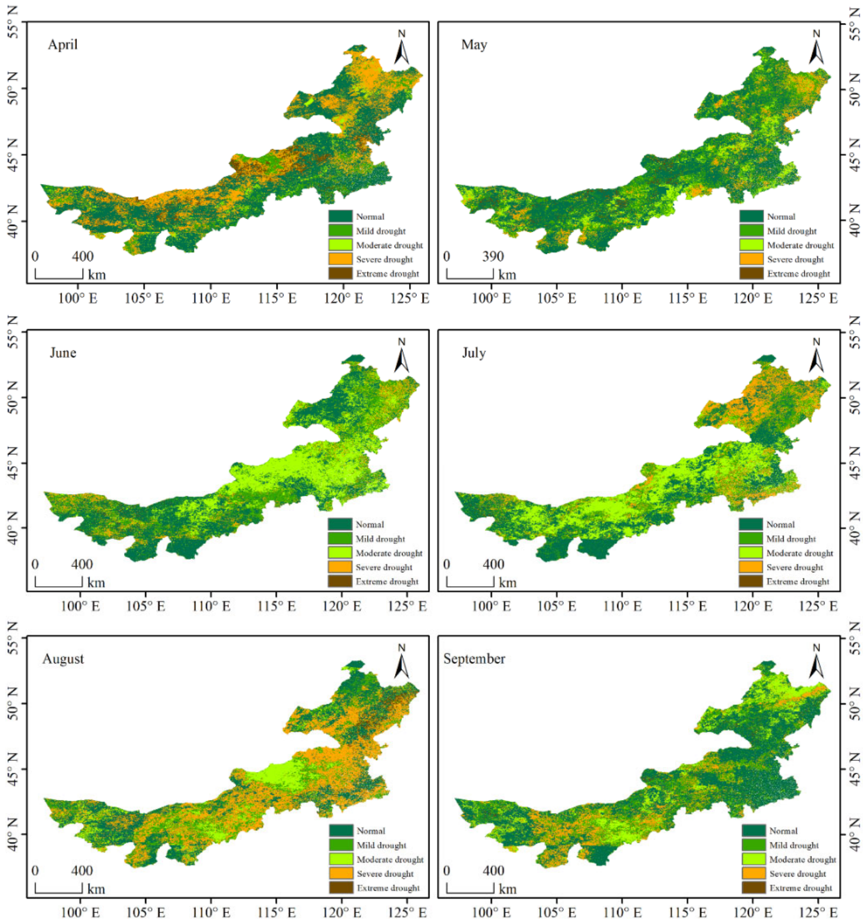

Figure 4. Monitoring results of the drought model during the growing season in 2012.

4.2.2. Analysis of Grassland Drought Monitoring Model Monitoring Results in Normal Years

We monitored and classified the drought from April to September 2015 using the constructed grassland drought monitoring model (Figure 5). In April, except for moderate or extreme drought in eastern Inner Mongolia, most of Inner Mongolia was largely drought-free. In May, in general, there was an increased severity of drought, with moderate and severe droughts occurring in most areas. Severe drought appeared in some areas of northeastern Inner Mongolia, and extreme drought occurred in some central regions. Overall, drought had a tendency to decrease in severity, and mild drought and moderate drought appeared in most areas. Severe drought mainly appeared in some areas of northeastern Inner Mongolia, and there was no extreme drought in Inner Mongolia in June. In July, the drought conditions intensified, resulting in widespread moderate and extreme drought in most parts of Inner Mongolia. In August, the drought showed a decrease in severity, resulting in a large area of the drought diminishing. Overall, severe drought was mainly concentrated in the central regions of Inner Mongolia. Meanwhile, no drought occurred in the eastern regions of Inner Mongolia. In September, the drought in most areas had basically ceased. There was essentially no drought in most regions, except for moderate or severe drought in some areas of Inner Mongolia.

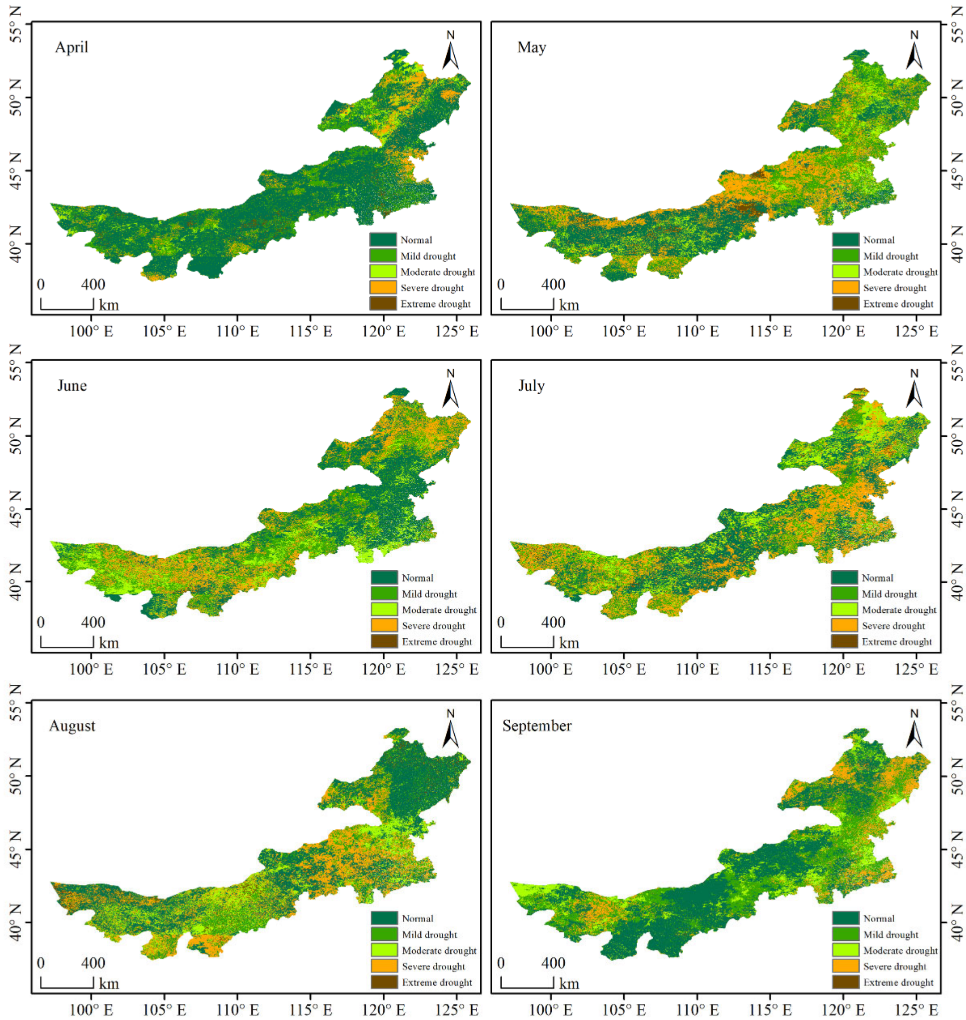

Figure 5. Monitoring results of the drought model during the growing season in 2015.

4.2.3. Analysis of Grassland Drought Monitoring Model Monitoring Results in Dry Years

From April to September 2017, the grassland drought monitoring model constructed in this study was used to monitor and classify the grassland drought in Inner Mongolia. As shown in Figure 6, there was essentially no extreme drought in Inner Mongolia, and moderate drought occurred mainly in some areas of eastern Inner Mongolia in April. In May, the drought intensified, resulting in widespread severe and extreme drought in most areas of Inner Mongolia, and extreme drought in some areas. In June, extreme drought had a tendency to decrease in severity in Inner Mongolia. Except for severe drought in eastern Inner Mongolia, mild drought and moderate drought occurred in most areas of Inner

Mongolia. In August, overall, mild drought occurred in most regions of Inner Mongolia, and severe drought intensified in the central regions of Inner Mongolia. In September, the drought intensified, resulting in widespread moderate and severe drought in most parts of Inner Mongolia, and even extreme drought in some areas.

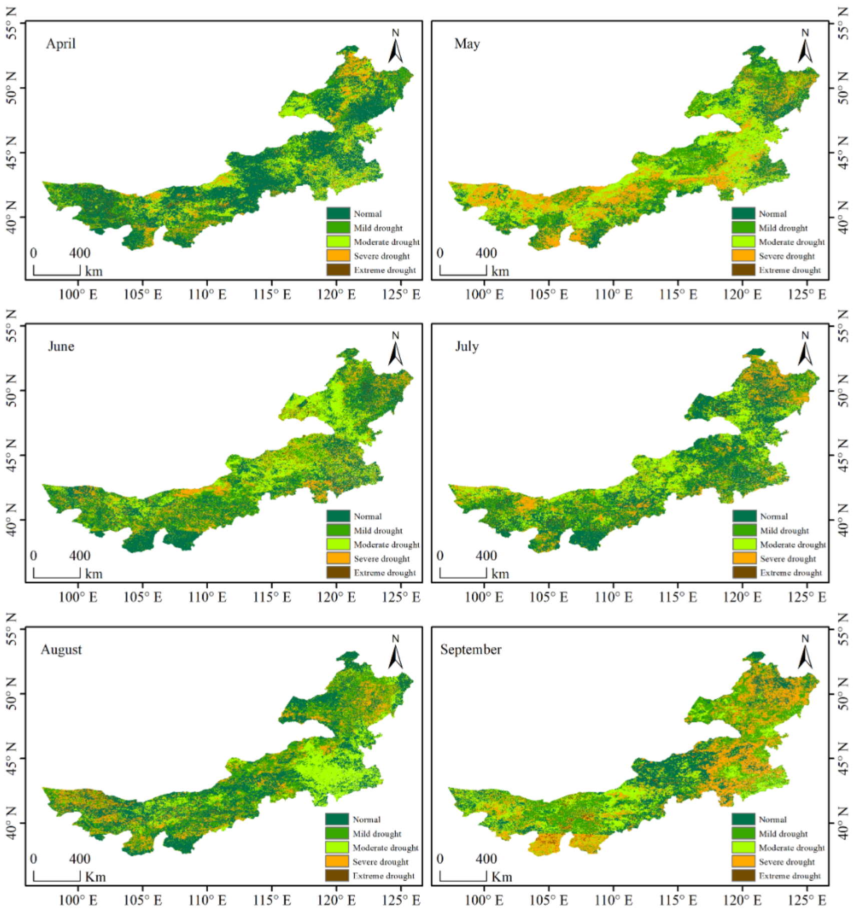

Figure 6. Monitoring results of the drought model during the growing season in 2017.

5. Discussion

To verify the accuracy and reliability of the monitoring results of the constructed grassland drought monitoring model, we compared the monitoring results of the model constructed in this study with the actual drought occurrence in the corresponding years (2012, 2015, and 2017), respectively.

According to the 2013 China Meteorological Disaster Yearbook, there were approximately 1,464,600 people affected by drought in Inner Mongolia in 2012. Approximately 431,000 people had difficulty gaining drinking water, and the no-harvest area was 11,000 hectares [40]. Overall, rangelands and pastures in Inner Mongolia suffered from different degrees of drought disaster. Except for the eastern part of Inner Mongolia, the temperature in April was approximately 1 °C higher than in the same period in normal years. A previous study proved that the precipitation in eastern Inner Mongolia was more than 80% less than in normal years [40]. The drought in most regions of Inner Mongolia was more serious in April due to high temperatures and low precipitation. In May, the temperature was approximately 1~2 °C higher than the temperature in the same month in normal years. At the same time, the precipitation was 130% to 200% higher than the precipitation in the same month in normal years. As a result, the drought that occurred in Inner Mongolia was somewhat less severe in May compared to April. The drought extent and spatial distribution of April and May in Inner Mongolia monitored by the drought monitoring model are highly similar to the occurrences of the actual recorded drought conditions. Additionally, the monitoring results of the model constructed in this study are consistent with the drought distribution in Inner Mongolia founded by Duan et al. (2013) [41]. These results indicate that the monitoring results of the model constructed in this study are objective and credible.

The temperature in central Inner Mongolia was approximately 1~2 °C lower than the temperature in the same month in normal years, while the temperature in western Inner Mongolia was approximately 1~2 °C higher than in the same period in normal years, or even more than 2 °C higher [40]. At the same time, heavy rainfall and even flooding occurred in 11 leagues (cities) in Inner Mongolia in June. In July, the temperature in central Inner Mongolia was slightly lower than the temperature in the same month in normal years, and the temperature in northeastern Inner Mongolia was 1~2 °C higher than in the same period in normal years. At the same time, the precipitation in most regions of Inner Mongolia was 130% to 200% times higher than in the same period in normal years. If only the effects of temperature and precipitation on drought are considered, Inner Mongolia as a whole would be drought-free in June or July [40]. In contrast, the monitoring results of the grassland drought monitoring model constructed in this study show that the drought conditions in Inner Mongolia in June and July were alleviated, but there were still different levels of drought disasters. These differences can be explained by the adaptation of regional vegetation to the regional environment during long-term growth. This makes grassland vegetation respond to drought with a certain lag. In addition to temperature and precipitation, the growing conditions of vegetation are affected by other natural hazards, such as floods, fire, storms, and lightning [42,43]. According to the Inner Mongolia Disaster Yearbook, in 2012, 12 leagues (cities) in Inner Mongolia experienced heavy rainfall, lightning storms, and strong convection storms [40]. From 20–28 June of the same year, Inner Mongolia suffered heavy localized rainfall, and some areas were hit by torrential rains, causing severe flooding. In addition, Inner Mongolia had the most serious grassland fire of the last 10 years. Since the drought monitoring model was constructed using the EVI as one of the model parameters, other natural disasters besides drought may also lead to a reduction in the EVI. Therefore, to a certain extent, the results of the drought monitoring model may differ from the actual drought conditions.

In general, high temperatures and low precipitation are the main reasons for the formation of regional drought. In August, the temperature in northeastern Inner Mongolia was slightly lower than in the same period in normal years. The temperature in the west was approximately 1 to 2 °C higher than the temperature in the same month in normal years. In addition, the precipitation in most regions was 30% to 50% lower than that in the same month in normal years. In September, the temperature in the west was approximately 1 °C higher than the temperature in the same month in a normal year. At the same time, the precipitation was less than the precipitation in the same month in normal years. Therefore, there was a drought disaster in Inner Mongolia in August and September, which is consistent with the drought monitoring model monitoring results. With the above analysis process, the RF-based grassland drought monitoring model established in this study can be used to monitor the spatial and temporal evolution of the drought process in Inner Mongolia. The results of the study are basically consistent with the actual drought conditions in 2012, indicating that the model has strong monitoring capability for wet years.

To verify the accuracy and reliability of the monitoring results of the grassland drought monitoring model in a normal year, we compared the monitoring results of the model constructed in this study with the actual drought occurrence in 2015. Previous studies have proven that mild drought and moderate drought were the mainly occurring drought disaster, and severe drought occurred only in some regions of Inner Mongolian in March and April of 2015 [44,45]. From June to August, there was mild drought or even severe drought in most regions of Inner Mongolia, and severe drought and extreme drought occurred in some areas. In September, drought occurred similarly to that in the summer. Even some areas of Inner Mongolia experienced extreme drought [46]. Through the above analysis process, the RF-based grassland drought monitoring model established in this study was used to monitor the spatial and temporal evolution of the drought process in Inner Mongolia. The results of the study are basically consistent with the actual drought conditions in 2015, suggesting that the model has a strong monitoring capability for normal years.

To verify the accuracy and reliability of the monitoring results of the grassland drought monitoring model in dry years, we compared the monitoring results of the model constructed in this study with the actual drought occurrence in 2017. According to the 2018 China Meteorological Disaster Yearbook, Inner Mongolia experienced a spring–summer drought in 2017 [47,48]. From March to June, the precipitation in most regions was 50% lower than in the same period in normal years. Severe drought to extreme drought mainly occurred in the eastern part of Inner Mongolia. The drought area accounted for 61% of the total Inner Mongolia area in spring. In July, high temperatures and low precipitation occurred in most regions of Inner Mongolia, resulting in drought disasters in most regions. Drought decreased in severity in August, and drought spread throughout central Inner Mongolia. The results are basically in agreement with the actual drought conditions in 2017. In addition, the monitoring results of the present model are consistent with the monitoring results of the spatial variation characteristics of the 2017 drought in Inner Mongolia based on the 16 d timescale analysis [38], illustrating that the model has a strong monitoring capability for drought years.

Combined with the above analysis process, the results of the model in this study are basically in accordance with the actual drought conditions in wet years, normal years, and dry years, suggesting that the model has a strong monitoring capability in Inner Mongolia. In other words, the RF-based grassland drought monitoring model developed in this study can be used to monitor the temporal and spatial evolution of drought processes in Inner Mongolia.

The model constructed in this study still has some limitations and needs to be improved. Human activities are increasingly contributing to the severity, frequency, and negative impacts of drought disasters. Therefore, we will take human activities into account in the construction of drought monitoring models in future work.

6. Conclusions

Drought processes are related to numerous factors, such as the atmosphere, soil, and vegetation. To describe and estimate drought conditions more accurately, we should consider a combination of drought-induced factors, including soil, water, and vegetation growth conditions. In this study, the precipitation state index (GPMI), temperature state index (TCI), enhanced vegetation state index (EVI), aspect, and slope direction and elevation were used as model-independent variable datasets. SPEI6 was used as a model-dependent variable dataset. We used multi-source spatial data (site data and remote sensing data) and random forests to synthesize the effects of multiple drought factors on drought. A grassland drought monitoring model based on random forest was constructed. The results of this study are summarized below.

(1) The grassland drought monitoring model established in this study can quantitatively monitor the drought condition of the Inner Mongolia grassland. The correlation coefficient (R) between the drought level obtained from the model training set and the measured SPEI6 reached 0.9706, and the correlation coefficient between the drought level obtained from the model test set and the measured SPEI6 reached 0.6387.

(2) The grassland drought monitoring model can objectively describe the degree of drought in the Inner Mongolia grassland. The correlation coefficient between the grassland drought index and the standardized precipitation evapotranspiration index (SPEI) from the model was 87.90%, demonstrating that the model can be used for drought monitoring and early warning of grassland drought in Inner Mongolia.

(3) In this study, drought events from April to September in Inner Mongolia were monitored in wet years, normal years, and dry years, using the constructed model. The monitoring results of the model constructed in this study were in accordance with the actual

drought occurrence degree and spatial distribution. Therefore, the model constructed in this study has a strong monitoring capability for grassland drought disasters.

Author Contributions: Conceptualization, Q.W. and L.Z.; software, Q.W. and W.Z.; methodology, Q.W. and M.W.; resources, J.W. and M.D.; writing—review and editing, Q.W. and Q.Z. All authors have read and agreed to the published version of the manuscript.

Funding: This study was supported by the Natural Science Foundation of China (32060279), Natural Science Foundation of Shandong Province (ZR2022MD063), and the Doctoral Startup Foundation of Liaocheng University (318052036, 318052116).

Data Availability Statement: Data will be made available upon request.

Conflicts of Interest: The authors declare no conflict of interest.

References

1. Orimoloye, I.R.; Belle, J.A.; Ololade, O.O. Drought disaster monitoring using MODIS derived index for drought years: A space-based information for ecosystems and environmental conservation. *J. Environ. Manag.* **2021**, *284*, 112028. [CrossRef] [PubMed]
2. Wang, Q.; Liu, Y.Y.; Zhang, Y.Z.; Tong, L.J.; Sun, Z. Assessment of Spatial Agglomeration of Agricultural Drought Disaster in China from 1978 to 2016. *Sci. Rep.* **2019**, *9*, 14393. [CrossRef] [PubMed]
3. Othman, D.B.; Abida, H. Monitoring and mapping of drought in a semi-arid region: Case of the Merguellil watershed, central Tunisia. *Environ. Monit. Assess.* **2022**, *194*, 287. [CrossRef] [PubMed]
4. Zhang, Y.; Wang, Q.; Wang, Z.; Yang, Y.; Li, J. Impact of human activities and climate change on the grassland dynamics under different regime policies in the Mongolian Plateau. *Sci. Total Environ.* **2019**, *698*, 134304. [CrossRef]
5. Balti, H.; Abbes, A.B.; Mellouli, N.; Farah, I.R.; Lamolle, M. A review of drought monitoring with big data: Issues, methods, challenges and research directions. *Ecol. Inform.* **2020**, *60*, 101136. [CrossRef]
6. Azam, M.; Hunjra, A.I.; Bouri, E.; Tan, Y.; Al-Faryan, M. Impact of institutional quality on sustainable development: Evidence from developing countries. *J. Environ. Manag.* **2021**, *298*, 113465. [CrossRef]
7. Askarimarnani, S.S.; Kiem, A.S.; Twomey, C.R. Comparing the performance of drought indicators in Australia from 1900 to 2018. *Int. J. Climatol.* **2020**, *41*, E912–E934. [CrossRef]
8. Mukherjee, S.; Mishra, A.; Trenberth, K.E. Climate Change and Drought: A Perspective on Drought Indices. *Curr. Clim. Chang. Rep.* **2018**, *4*, 145–163. [CrossRef]
9. Zhou, J.; Chen, X.; Xu, C.; Wu, P. Assessing Socioeconomic Drought Based on a Standardized Supply and Demand Water Index. *Water Resour. Manag.* **2022**, *36*, 1937–1953. [CrossRef]
10. Benedict, T.D.; Brown, J.F.; Boyte, S.P.; Howard, D.M.; Evenson, K.A. Exploring VIIRS Continuity with MODIS in an Expedited Capability for Monitoring Drought-Related Vegetation Conditions. *Remote Sens.* **2021**, *13*, 1210. [CrossRef]
11. Chen, C. Review of Drought Disaster Evaluation. *Prog. Geogr.* **2011**, *30*, 891–898.
12. Svoboda, M.; Fuchs, B.; Darani, S.M.M. *Handbook of Drought Indicators and Indices*; WMO: Geneva, Switzerland, 2016.
13. Qi, L.A.; Sha, Z.A.; Hz, C.; Yun, B.A.; Jza, B. Monitoring drought using composite drought indices based on remote sensing. *Sci. Total Environ.* **2020**, *711*, 134585.
14. Rhee, J.; Im, J.; Carbone, G.J. Monitoring agricultural drought for arid and humid regions using multi-sensor remote sensing data. *Remote Sens. Environ.* **2010**, *114*, 2875–2887. [CrossRef]
15. Shen, R.; Huang, A.; Li, B.; Guo, J. Construction of a drought monitoring model using deep learning based on multi-source remote sensing data. *Int. J. Appl. Earth Obs. Geoinf.* **2019**, *79*, 48–57. [CrossRef]
16. Hao, Z.; Aghakouchak, A. Multivariate Standardized Drought Index: A parametric multi-index model. *Adv. Water Resour.* **2013**, *57*, 12–18. [CrossRef]
17. Kim, S.W.; Jung, D.; Choung, Y.J. Development of a Multiple Linear Regression Model for Meteorological Drought Index Estimation Based on Landsat Satellite Imagery. *Water* **2020**, *13*, 3393. [CrossRef]
18. Lee, Y. Development of Integrated Crop Drought Index by Combining Rainfall, Land Surface Temperature, Evapotranspiration, Soil Moisture, and Vegetation Index for Agricultural Drought Monitoring. *Remote Sens.* **2021**, *13*, 1778. [CrossRef]
19. Breiman, L. Random forest. *Mach. Learn.* **2001**, *45*, 5–32. [CrossRef]
20. Svetnik, V. Random forest: A classification and regression tool for compound classification and QSAR modeling. *J. Chem. Inf. Comput. Sci.* **2003**, *43*, 1947–1958. [CrossRef]
21. Ham, J.; Chen, Y.; Crawford, M.M.; Ghosh, J. Investigation of the random forest framework for classification of hyperspectral data. *IEEE Trans. Geosci. Remote Sens.* **2005**, *43*, 492–501. [CrossRef]
22. Rodriguez-Galiano, V.F.; Ghimire, B.; Rogan, J.; Chica-Olmo, M.; Rigol-Sanchez, J.P. An assessment of the effectiveness of a random forest classifier for land-cover classification. *ISPRS J. Photogramm. Remote Sens.* **2012**, *67*, 93–104. [CrossRef]

23. Shimizu, K.; Ota, T.; Mizoue, N.; Yoshida, S. A comprehensive evaluation of disturbance agent classification approaches: Strengths of ensemble classification, multiple indices, spatio-temporal variables, and direct prediction. *ISPRS J. Photogramm. Remote Sens.* **2019**, *158*, 99–112. [CrossRef]
24. Speiser, J.L.; Miller, M.E.; Tooze, J.; Ip, E. A comparison of random forest variable selection methods for classification prediction modeling. *Expert Syst. Appl.* **2019**, *134*, 93–101. [CrossRef]
25. Fang, A.; Bao, M.; Chen, W.; Dong, J. Assessment of Surface Ecological Quality of Grassland Mining Area and Identification of Its Impact Range. *Nat. Resour. Res.* **2021**, *30*, 3819–3837. [CrossRef]
26. Van Der Heijden, M.G.; Klironomos, J.N.; Ursic, M.; Moutoglis, P.; Streitwolf-Engel, R.; Boller, T.; Wiemken, A.; Sanders, I.R. Mycorrhizal fungal diversity determines plant biodiversity, ecosystem variability and productivity. *Nature* **1998**, *396*, 69–72. [CrossRef]
27. Wang, Q.; Liu, X.; Wang, Z.; Zhao, L.; Zhang, Q.P. Time scale selection and periodicity analysis of grassland drought monitoring index in Inner Mongolia. *Glob. Ecol. Conserv.* **2022**, *36*, e02138. [CrossRef]
28. Zhao, G.; Han, Y.; Liu, M.; Zhao, S.; Liu, W. Characteristics of temporal and spatial variations of extreme temperature events in Inner Mongolia during 1951–2014. *J. Arid Land Resour. Environ.* **2017**, *31*, 110–116.
29. Yang, H.; Zhou, W.; Huang, L. Temporal and spatial patterns of grassland coverage and responses to hydrothermic factors in Inner Mongolia from 2001 to 2016. *Pratacultural Sci.* **2019**, *36*, 359–367.
30. Ai-Hua, M.; Yue, D.P.; Zhao, J.B.; Qian, H.U. Spatiotemporal Variation and Effect of Extreme Precipitation in Inner Mongolia in Recent 60 Years. *Arid Zone Res.* **2020**, *37*, 74–85.
31. Zarei, A.R.; Moghimi, M.M. Modified version for SPEI to evaluate and modeling the agricultural drought severity. *Int. J. Biometeorol.* **2019**, *63*, 911–925. [CrossRef]
32. Vicent Serrano, S.M.; Beguería, S.; López Moreno, J.I. A Multiscalar Drought Index Sensitive to Global Warming: The Standardized Precipitation Evapotranspiration Index. *J. Clim.* **2010**, *23*, 1696–1718. [CrossRef]
33. Singh, R.P.; Roy, S.; Kogan, F. Vegetation and temperature condition indices from NOAA AVHRR data for drought monitoring over India. *Int. J. Remote Sens.* **2003**, *24*, 4393–4402. [CrossRef]
34. Ba, R.; Song, W.; Lovallo, M.; Zhang, H.; Telesca, L. Informational analysis of MODIS NDVI and EVI time series of sites affected and unaffected by wildfires. *Phys. A Stat. Mech. Appl.* **2022**, *604*, 127911. [CrossRef]
35. Patasaraiya, M.K.; Devi, R.M.; Sinha, B.; Bisaria, J.; Saran, S.; Jaiswal, R. Understanding the Resilience of Sal and Teak Forests to Climate Variability Using NDVI and EVI Time Series. *For. Sci.* **2021**, *67*, 192–204. [CrossRef]
36. Enebish, B.; Dashkhuu, D.; Renchin, M.; Russell, M.; Singh, P. Impact of Climate on the NDVI of Northern Mongolia. *J. Indian Soc. Remote Sens.* **2019**, *48*, 333–340. [CrossRef]
37. Qin, Y.; Zhang, T.-B.; Yi, G.-H.; Wei, P.-T.; Yang, D. Remote sensing monitoring and analysis of influencing factors of drought in Inner Mongolia growing season since 2000. *J. Nat. Resour.* **2021**, *36*, 459–475. [CrossRef]
38. Kogan, F.N. Application of vegetation index and brightness temperature for drought detection. *Adv. Space Res.* **1995**, *15*, 91–100. [CrossRef]
39. Wang, S.; Wang, S.; Feng, J. Drought Events and Its causes in Autumn of 2012 in China. *J. Arid Meteorol.* **2012**, *30*, 660–666.
40. Duan, H.; Wang, S.; Feng, J. Drought Events and Its Causes in 2012 in China. *J. Arid Meteorol.* **2013**, *31*, 220–229.
41. Krellenberg, K.; Müller, A.; Schwarz, A.; Höfer, R.; Welz, J. Flood and heat hazards in the Metropolitan Region of Santiago de Chile and the socio-economics of exposure. *Appl. Geogr.* **2013**, *38*, 86–95. [CrossRef]
42. Vorkauf, M.; Kahmen, A.; Krner, C.; Hiltbrunner, E. Flowering phenology in alpine grassland strongly responds to shifts in snowmelt but weakly to summer drought. *Alp. Bot.* **2021**, *131*, 73–88. [CrossRef]
43. Wang, S.; Wang, S.; Feng, J. Drought Events and Its Causes in 2015 in China. *J. Arid Meteorol.* **2016**, *34*, 382–389.
44. Zhang, Y.; Wang, S.; Feng, J. Drought Events and Its causes in Autumn of 2015 in China. *J. Arid Meteorol.* **2015**, *33*, 1050–1057.
45. Wang, S.; Zhang, Y.; Feng, J. Drought Events and Its causes in Summer of 2015 in China. *J. Arid Meteorol.* **2015**, *33*, 888–893.
46. Wang, S.; Wang, S.; Feng, J. Drought Events and Its causes in Autumn of 2017 in China. *J. Arid Meteorol.* **2017**, *35*, 1084–1089.
47. Zhang, Y.; Zhang, L.; Wang, S.; Feng, J. Drought Events and Its causes in Summer of 2017 in China. *J. Arid Meteorol.* **2017**, *33*, 899–905.
48. Zhang, Y.; Wang, S.; Feng, J. Drought Events and Its Causes in 2017 in China. *J. Arid Meteorol.* **2018**, *036*, 331–338.